RSC Advances

PAPER

View Article Online
View Journal | View Issue

Cite this: *RSC Adv.*, 2025, **15**, 49165

First-principles investigation of structural, elastic, electronic, thermodynamic, and optical properties of KBi_3 for optoelectronic applications

M. M. Rabbi[a] and Mst. A. Khatun *[b]

KBi_3, a recently explored non-layered cubic compound, offers a distinctive platform beyond conventional van der Waals-type materials due to its intriguing physical characteristics. In this study, we conduct a comprehensive first-principles density functional theory (DFT) investigation of its structural, elastic, electronic, thermodynamic, and optical properties to establish its potential for optoelectronic applications. The computed elastic constants satisfy Born stability criteria, and complementary mechanical indicators—including Pugh's ratio, Poisson's ratio, and Cauchy pressure—confirm the ductile and mechanically stable nature of KBi_3. The electronic band structure and density of states demonstrate metallic behavior with finite states at the Fermi level, accompanied by anisotropic energy dispersion that reflects variation in carrier effective mass along different crystallographic directions. Thermodynamic analysis within the quasi-harmonic Debye model predicts a relatively low Debye temperature, moderate melting point, and reduced lattice thermal conductivity, suggesting limited heat transport. Meanwhile, the optical spectra reveal pronounced reflectivity in the infrared region, a high refractive index, and strong absorption spanning the visible-ultraviolet range, underscoring the compound's metallic character and multifunctional optical response. These findings provide the first detailed theoretical framework for KBi_3 and highlight its promise as a candidate material for advanced optoelectronic device technologies.

Received 20th September 2025
Accepted 2nd December 2025

DOI: 10.1039/d5ra07125a

rsc.li/rsc-advances

1 Introduction

The search for novel intermetallic compounds with multifunctional physical properties has gained significant momentum in recent years due to their wide-ranging applications in optoelectronic, thermal, and photonic technologies. Among these, bismuth-based materials have attracted exceptional interest because of their heavy-element electronic structure, strong spin–orbit coupling, and unique lattice dynamics, which together enable tunable electronic, thermal, and optical behaviors.[1–5] Compounds containing bismuth often exhibit metallic conductivity, low lattice thermal conductivity, and high infrared reflectivity, features desirable for energy-efficient coatings, infrared mirrors, and next-generation photonic devices.[6–8] Despite substantial progress in understanding Bi-based systems such as $SrBi_3$, $BaBi_3$, $LaBi_3$, and KBi_2, the newly discovered KBi_3 compound, crystallizing in the $AuCu_3$-type cubic structure, remains largely unexplored from a theoretical standpoint.[2,6,8,9] A systematic first-principles study of KBi_3 is therefore essential to uncover the microscopic origins of its mechanical stability, metallic behavior, and optical response, thereby expanding the fundamental understanding of alkali–bismuth intermetallics and guiding their potential integration into advanced optoelectronic applications.

The selection of KBi_3 for this investigation is driven by its distinct structural and electronic characteristics compared to other members of the Bi-based intermetallic family. Unlike KBi_2 or $RbBi_2$, which crystallize in the Laves phase structure and exhibit conventional metallic bonding, KBi_3 adopts a non-layered $AuCu_3$-type cubic framework, a configuration rarely observed among alkali–bismuth systems.[2,6,9] This structural uniqueness arises from the three-dimensional K–Bi network, which allows for enhanced orbital hybridization and anisotropic carrier transport, properties that are often associated with functional metallic materials suitable for infrared reflective and optoelectronic applications.[7,10,11] Furthermore, high-pressure synthesis and machine-learning-assisted crystal discovery have recently enabled the identification of KBi_3 as a stable phase with unusual diffraction signatures and potential for exotic physical behavior.[2] However, despite its experimental recognition, no comprehensive theoretical study has yet explored its elastic, electronic, thermodynamic, or optical properties, leaving a critical gap in understanding its structure–property correlations. Therefore, the present work aims to provide the first integrated first-principles framework for KBi_3, clarifying how its atomic arrangement governs its mechanical robustness, metallic conductivity, and multifunctional optical performance.

[a]*Department of Physics, University of Rajshahi, Rajshahi-6205, Bangladesh*
[b]*Department of Physics, Hajee Mohammad Danesh Science and Technology University, Dinajpur-5200, Bangladesh. E-mail: asma@tch.hstu.ac.bd*

In light of these considerations, the present study delivers a comprehensive first-principles analysis of KBi_3, addressing the absence of theoretical data on its mechanical stability, electronic band characteristics, thermodynamic response, and optical behavior. By integrating density functional theory (DFT) with the quasi-harmonic Debye model and optical response calculations, this work provides a multidimensional understanding of KBi_3 that extends beyond prior studies on related Bi-based intermetallics.[9,12–14] The investigation also aligns with recent advances in data-driven materials discovery and high-throughput DFT simulations, which have accelerated the identification of new compounds for optoelectronic and energy applications.[7,15,16] Recent research highlights that metallic Bi-based frameworks can exhibit low lattice thermal conductivity, high reflectivity, and strong absorption in the visible-UV range, properties that are central to the design of infrared coatings, thermal barrier materials, and photonic devices.[10,11,17] Therefore, elucidating the structure–property–function correlations of KBi_3 not only fills a major knowledge gap but also contributes to the broader understanding of alkali–bismuth intermetallics as potential multifunctional materials for next-generation optoelectronic and energy-efficient technologies.

2 Computational methodologies

The full-potential linearized augmented plane wave approach with local orbitals (FP-LAPW+lo), as implemented in the WIEN2k software package,[18] was used in this study's computations within the context of density functional theory (DFT). The generalized gradient approximation (GGA) contained in WIEN2k was parameterized using the Perdew–Burke–Ernzerhof (PBE) method for structural optimization.[19,20] The muffin-tin radii (RMT) were determined to be 2.5 a.u. for the K atom and 2.5 a.u. for Bi. The plane wave cutoff value RK_{max} was set at 8.0 to guarantee accurate results; R stands for the smallest RMT, and K_{max} is the reciprocal lattice vector's maximum modulus. Using a dense 21 × 21 × 21 Monkhorst–Pack k-point mesh without shifting, Brillouin zone integrations were carried out. The energy and charge convergence criteria were established at 10^{-4} Ry and 0.001e, respectively. The CASTEP code[21] was employed to calculate the phonon dispersion and elastic constants. For these calculations, the first irreducible Brillouin zone (BZ) was sampled using a 12 × 12 × 12 Monkhorst–Pack k-point grid, and a plane-wave cutoff energy of 450 eV was applied for the KBi_3 compound.

The energy-dependent optical constants were computed by evaluating the electronic transition probabilities between various energy bands. The imaginary part of the complex dielectric function, denoted as $\varepsilon_2(\omega)$, was derived using the momentum matrix elements between the occupied and unoccupied electronic states within the valence and conduction bands, respectively. This was accomplished using the formulation implemented in CASTEP and is expressed as follows:

$$\varepsilon_2(\omega) = \frac{2e^2\pi}{\Omega\varepsilon_0}\sum_{k,v,c}\left|\psi_k^c|\hat{u}.\boldsymbol{r}|\psi_k^v\right|^2\delta\left(E_k^c - E_k^v - \hbar\omega\right) \quad (1)$$

Here, e is the elementary charge, ε_0 is the permittivity of free space, and $\hbar$ is the reduced Planck constant. Ω denotes the unit cell volume, while ω is the angular frequency of the incident electromagnetic radiation. The symbols ψ_k^c and ψ_k^v represent the conduction and valence band wavefunctions at a given k-point, respectively. The term $\hat{u}$ denotes the unit vector along the polarization direction of the incident electric field, and r is the position operator appearing in the dipole transition matrix element $\langle\psi_k^c|\hat{u}\cdot r|\psi_k^v\rangle$. The Dirac delta function $\delta(E_k^c - E_k^v - \hbar\omega)$ ensures conservation of energy during optical transitions.

The real part of the dielectric function, $\varepsilon_1(\omega)$, was obtained from $\varepsilon_2(\omega)$ *via* Kramers–Kronig transformations. While $\varepsilon_1(\omega)$ describes the material's electric polarization response, $\varepsilon_2(\omega)$ is directly related to the optical absorption characteristics.[22,23] Once $\varepsilon_1(\omega)$ and $\varepsilon_2(\omega)$ are determined, other frequency-dependent optical parameters—such as refractive index, extinction coefficient, reflectivity, and absorption coefficient—can be systematically calculated. This methodology has been widely validated and employed in numerous previous studies for the accurate prediction of the optical properties of crystalline materials.[24–28]

The Gibbs2 (ref. 29) software employs a quasi-harmonic Debye model to calculate the equilibrium state for a given pressure and temperature (p, T) is determined, other thermodynamic properties can be calculated using the corresponding equilibrium volume in the relevant thermodynamic formulas. For example, bulk modulus (B), Debye temperature (θ_D), heat capacities (C_v,C_p), and volumetric thermal expansion coefficient (α).

For an isotropic solid, the Debye temperature θ_D is expressed as:[30]

$$\theta_D = \frac{\hbar}{K}\left[6\pi^2 V^{\frac{1}{2}} n\right]^{\frac{1}{3}} \cdot f(\sigma)\sqrt{\frac{B_s}{M}} \quad (2)$$

where $\hbar$ is the reduced Planck's constant, k_B is the Boltzmann constant, V is the molecular volume per formula unit, and n represents the number of atoms per formula unit. The term $f(\sigma)$ is a function of Poisson's ratio (σ) that accounts for the material's elastic anisotropy, B_s denotes the adiabatic bulk modulus, and M is the molecular mass per unit cell and $f(\sigma)$ is given by[31,32]

$$f(\sigma) = \left\{3\left[2\left(\frac{2}{3}\cdot\frac{1+\sigma}{1-2\sigma}\right)^{\frac{3}{2}} + \left(\frac{1}{3}\cdot\frac{1+\sigma}{1-\sigma}\right)^{\frac{3}{2}}\right]^{-1}\right\}^{\frac{1}{3}} \quad (3)$$

Since B_s measures the compressibility of the crystal for fixed quantum state populations, it can be approximated by the static compressibility. The static compressibility is given by:[30]

$$B_s = B(V) = V\frac{d^2E(V)}{dV^2} \quad (4)$$

The heat capacities, C_v and C_p are given as follows:[30]

$$C_{v,vib} = 3nk\left[4D\left(\frac{\theta_D}{T}\right) - \frac{3\theta_D/T}{e^{\theta_D/T}-1}\right] \quad (5)$$

$$C_{p,vib} = C_{v,vib}(1 + \alpha\gamma T) \quad (6)$$

Finally, the thermal expansion (α) is given by:

$$\alpha = \frac{\gamma C_{v,vib}}{B_T V} \quad (7)$$

here, the subscripts v is for volume, p is for pressure, vib for vibrational, T for temperature. and,

$C_{v,vib}$ = Vibrational heat capacity at constant volume, derived from the Debye model. $C_{p,vib}$ = Vibrational heat capacity at constant pressure, incorporating thermal expansion. γ = Grüneisen parameter. B_T = Isothermal bulk modulus, representing resistance to volume change under isothermal compression.

3 Results and analysis

3.1 Structural and mechanical properties

The intermetallic compound KBi_3 crystallizes in a cubic structure with the $Pm\bar{3}m$ space group, which is centrosymmetric. Each unit cell contains one formula unit, totaling 4 atoms. In this structure, K atoms occupy the 1a Wyckoff position at (0.0, 0.0, 0.0), while Bi atoms are located at the 3c Wyckoff sites with coordinates (0.5, 0.0, 0.5): (0.5, 0.5, 0.0) and (0.0, 0.5, 0.5), respectively. The equilibrium lattice parameters and total energy were obtained through optimization using the Murnaghan equation of state:[33]

$$E(V) = E_0 + \frac{9V_0B_0}{16}\left\{\left[\left(\frac{V_0}{V}\right)^{\frac{2}{3}} - 1\right]^3 B_0' + \left[\left(\left(\frac{V_0}{V}\right)^{\frac{2}{3}} - 1\right)\right]^2\left[6 - 4\left(\frac{V_0}{V}\right)^{\frac{2}{3}}\right]\right\} \quad (8)$$

The calculated lattice parameters, summarized in Table 1, are compared with both available experimental data and previously published theoretical results. A good agreement is observed in both cases, validating the reliability of our approach. The equilibrium crystal structure of KBi_3 is shown in Fig. 1.

We determined the compound's cohesive and formation energies to confirm its thermodynamic stability even though it had been created experimentally. The formation energy ΔE_f of

Table 1 Calculated lattice constant a (in Å), equilibrium volume V (in Å^3) of the unit cell, minimum total energy E_0 (in eV), formation energy ΔE_f (in eV per atom), Cohesive energy E_{coh} (in eV per atom) of KBi_3 is compared with the previously reported theoretical value

Phase	a	V	E_0	ΔE_f	E_{coh}	Ref.
KBi_3	4.7123	104.64	−1233.54	−1.93	−3.45	This[a]
KBi_3	4.7638	108.11	—	—	—	2

[a] Refers to our theoretical investigation.

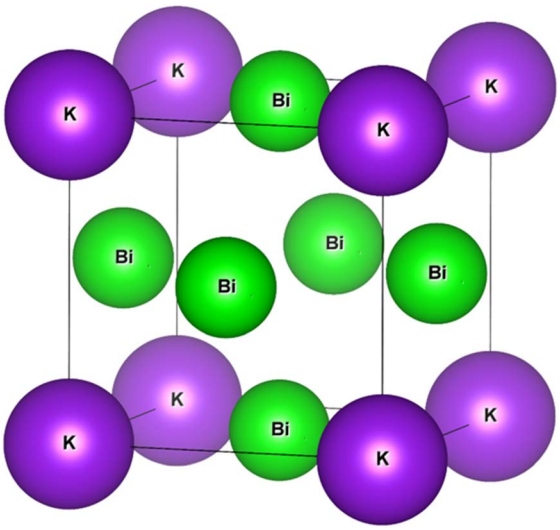

Fig. 1 Optimized equilibrium crystal structure of KBi_3.

KBi_3 at the ground state was calculated using the following expression:[34,35]

$$\Delta E_f(KBi_3)_{fu} = \frac{E_{tot}(KBi_3)_{fu} - E_s(K) - 3E_s(Bi)}{4} \quad (9)$$

where, $E_{tot}(KBi_3)_{fu}$ is the total energy of KBi_3 per formula unit and E_s(K) and E_s(Bi) represent the total energy of single atomic elements of K and Bi atoms, respectively.

Additionally, the cohesive energy (E_{coh}) was calculated by using the following expression:[36]

$$E_{coh} = -\frac{E_{tot}(KBi_3)_{fu} - n_K E(K) - n_{Bi}E(Bi)}{n_K + n_{Bi}} \quad (10)$$

where, $E_{tot}(KBi_3)_{fu}$ is the total energy of KBi_3 per formula unit and the terms n_K and n_{Bi} denote the number of K and Bi atoms in the unit cell. The calculated values of the formation energy and cohesive energy of the KBi_3 compound are presented in Table 1. The negative values confirm the thermodynamic stability of KBi_3, indicating that the compound is energetically favorable for synthesis under equilibrium conditions.

Understanding the structural integrity of crystalline materials requires an understanding of elastic stiffness constants. These constants offer vital information about how a crystal reacts to external mechanical stresses in addition to describing the mechanical and dynamical behavior of solids. As a result, they are essential for determining the mechanical strength of a material.[37] For cubic crystal systems, three independent elastic constants exist:[38,39] C_{11}, C_{12} and C_{44}. The elastic constants of KBi_3 that we determined during this investigation are shown in Table 2. The elastic moduli were then calculated using these constants. The determined elastic constants must meet the Born mechanical stability requirements in order to ensure mechanical stability[40] ($C_{11} > 0$, $C_{11} - C_{12} > 0$, $C_{44} > 0$, $(C_{11} + 2C_{12}) > 0$). All of these requirements are met by our calculated elastic constants, demonstrating the mechanical stability of KBi_3.

Table 2 Calculated elastic constants C_{ij} (in GPa), bulk modulus B (in GPa), shear modulus G (in GPa), Young's modulus Y (in GPa), Pugh's ratio B/G, poisson ratio ν, Cauchy pressure C_p, Kleinman parameter ζ and machinability index $\mu_M$for KBi_3 compound compared with related Bi-based intermetallic compounds

Compounds	C_{11}	C_{12}	C_{44}	B	G	Y	B/G	ν	C_p	ζ	μ_M	Ref.
KBi_3	70.30	45.60	20.00	53.80	16.40	44.80	3.28	0.36	25.60	0.75	2.69	This[a]
KBi_2	32.54	24.02	6.60	26.86	5.54	15.54	4.85	0.41	8.52	0.89	4.07	9
$RbBi_2$	50.93	20.74	17.81	30.80	16.73	42.37	1.85	0.27	30.19	0.57	1.73	9

[a] Refers to our theoretical investigation.

The polycrystalline elastic parameters bulk modulus (B), shear modulus (G), and Young's modulus (Y) were computed using the Voigt–Reuss–Hill (VRH) averaging scheme:[41–43]

$$\left.\begin{array}{c} B = B_H = (B_R + B_v)/2 \\ \text{and } G = G_H = G_R + G_v/2 \end{array}\right\} \quad (11)$$

The following expression was then used to compute Young's modulus (Y) and Poisson's ratio (ν) using the determined bulk modulus (B) and shear modulus (G):[44]

$$\left.\begin{array}{c} Y = \dfrac{9GB}{3B+G} \\ \text{and} \quad \nu = \dfrac{3B-2G}{2(3B+G)} \end{array}\right\} \quad (12)$$

A lower shear modulus (G) value in comparison to the bulk modulus (B) (Table 2) indicates that the shear modulus is the main determinant of the material's mechanical stability. Young's modulus (Y) is the ratio of tensile stress to strain, quantifies how resistant (stiff) an elastic material is to changes in length.[45,46] This modulus also serves as an indicator of the material's thermal shock resistance. The material's resilience to thermal shock is also indicated by this modulus. The Pugh's ratio B/G,[47,48] is frequently used to describe whether a material is brittle or ductile where the bulk modulus (B) shows resistance to fracture, the shear modulus (G) represents resistance to plastic deformation.[49] A material is considered ductile if $B/G > 1.75$, and brittle otherwise.[50] According to Pugh's criterion, KBi_3 with a B/G ratio of 3.28 is categorized as ductile, showing comparable behavior to KBi_2,[9] whereas $RbBi_2$ (ref. 9) indicates relatively lower ductility. A crystalline substance's bonding nature is also connected to Poisson's ratio (ν). The usual range of ν for solids subject to central forces is 0.25 to 0.5.[51] A significant ionic character in its bonding is implied by the computed Poisson's ratio of 0.36, which also shows that KBi_3 is ductile and contains central forces. A particular elastic constant's difference from another is known as the Cauchy pressure, or C_P, (C_{12}–C_{44}).[52] A ductile character is indicated by a positive C_P value, whereas brittleness is indicated by a negative value. According to this criterion, KBi_3 has a ductile nature, with KBi_3 more ductile than KBi_2 yet marginally less ductile than $RbBi_2$.[9] The internal strain parameter, also known as the Kleinman parameter (ζ), is another crucial mechanical parameter that we assessed. It is computed using the formula and measures a material's propensity for bond bending as opposed to bond stretching:[53]

$$\zeta = \frac{C_{11} + 8C_{12}}{7C_{11} + 2C_{12}} \quad (13)$$

This dimensionless parameter usually has a value between 0 and 1. Bond bending is more advantageous when the value is close to 1, whereas a value close to 0 indicates that bond stretching predominates. The calculated ζ value for KBi_3 was 0.75, indicating that bond bending plays a significant role in the compound's elastic response. This value lies between that of KBi_2 and $RbBi_2$,[9] suggesting that the bond-bending contribution in KBi_3 is more pronounced than in $RbBi_2$ but somewhat less dominant compared to KBi_2. The machinability index (μ_M) measures a solid's machinability by showing how easily it can be machined with cutting or shaping tools. The ease or difficulty of cutting, molding, or otherwise transforming the solid into different forms is estimated by this index. A material's machinability index (μ_M) can be written as:[54]

$$\mu_M = \frac{B}{C_{44}} \quad (14)$$

Additionally, a solid's plasticity and dry lubricating properties can be assessed using the machinability index (μ_M).[55–58] A greater μ_M value usually indicates superior dry lubricating performance, which is typified by reduced friction and improved plastic deformation capacity. The ratio is another helpful measure of dry lubricity and flexibility $\frac{B}{C_{44}}$. A larger $\frac{B}{C_{44}}$ value corresponds to reduced friction, higher lubrication efficiency, and greater plastic strain capacity. Interestingly, KBi_3 exhibits superior lubricating properties compared to the closely related bismuth-based compounds KBi_2 (ref. 9) and $RbBi_2$.[9] The values of Young's modulus (Y) and the elastic anisotropy parameter (C_{11}–C_{12}) can also be used to assess plasticity;[59] lower values of both Y and C_{11}–C_{12} suggest enhanced plasticity. Among these compounds, KBi_3 shows higher softness and ductility compared to KBi_2 and $RbBi_2$. These results indicate that KBi_3 demonstrates excellent softness and ductility, which are key qualities for the manufacturing of flexible conducting devices.

Another crucial thermophysical factor that restricts a material's use at high temperatures is its melting temperature, or T_m. The total bonding strength of solids is also reflected in T_m.

Bonding energy and melting point are related because stronger interatomic connections usually take more thermal energy to break, which raises the melting point of a material. High bonding energy materials in crystalline solids have higher melting points, which are indicative of their increased thermal stability and structural rigidity. Consequently, the melting point can be used as a proxy for bond strength and general thermal resistance. Using the empirical equation, one can determine the melting temperature, T_m, for KBi_3:[60]

$$T_m = [553 + (5.91\ \text{K GPa}^{-1})C_{11}] \pm 300 \quad (15)$$

The calculated T_m of KBi_3 is determined to be about 968.5 K, which is higher than that of KBi_2 (745.28 K) and $RbBi_2$ (853.99K),[9] as listed in Table 3. However, as is common with such computer predictions, this value has a substantial uncertainty of $\pm$ 300 K. The anticipated melting point indicates that KBi_3 has a good level of thermal stability, albeit the uncertainty range. Although the compound is stable in ambient settings, its relatively moderate T_m value suggests that it may tolerate high temperatures, which is crucial for any optoelectronic device applications.

The Debye temperature (θ_D), a basic property of crystals, is intimately associated with a number of important physical properties of solids, including melting temperature, phonon specific heat, and lattice thermal conductivity. The temperature at which all of a solid's vibrational (phonon) modes experience thermal excitation is known as the Debye temperature. It directly affects the material's thermal behavior and acts as a vibrational property indicator. Debye temperature (θ_D) is also linked to the material's sound speed and phonon density of states, is crucial in figuring out the crystal's heat capacity and thermal transport properties. A characteristic parameter of crystals, the Debye temperature is defined as follows in terms of mean velocity:[61]

$$\theta_D = \frac{h}{k_B}\left(\frac{3n}{4\pi V_0}\right)^{1/3} v_m \quad (16)$$

where V_0 is unit cell's volume, n is number of atoms in the unit cell, h is Planck's constant, and k_B is Boltzmann's constant. The crystal's mean sound velocity, or v_m, is given by:[61]

$$v_m = \left[\frac{1}{3}\left(\frac{2}{v_t^3} + \frac{1}{v_l^3}\right)\right]^{-1/3} \quad (17)$$

The longitudinal and transverse sound velocities, denoted by v_l and v_t, respectively, are derived from the following equations using the shear modulus G, bulk modulus B, and density ρ:

$$v_l = \sqrt{\frac{3B + 4G}{3\rho}} \text{ and } v_t = \sqrt{\frac{G}{\rho}} \quad (18)$$

The calculated θ_D of KBi_3 is 143.72 K, as shown in Table 3 is higher than that of KBi_2 (91.05 K) but slightly lower than $RbBi_2$ (147.65 K).[9] This relatively low θ_D indicates a soft lattice and weak interatomic bonding, which correspond to lower phonon frequencies and mechanical softness. Thus, the moderate Debye temperature of KBi_3 aligns well with its potential as a low-temperature conductor. The relatively low Debye temperature and average sound velocities reflect a soft lattice with slow phonons, which naturally enhances phonon–phonon scattering and thus suppresses the lattice thermal conductivity.

The Grüneisen parameter is a crucial thermophysical characteristic that characterizes the lattice anharmonicity. It is frequently used to investigate phase transitions involving volume changes and is essential to comprehending several basic physical characteristics, including sound absorption, heat conduction, thermal expansion, and the temperature dependence of elastic behavior. The strength of anharmonic interactions within a crystal lattice can also be inferred from this value. Low lattice anharmonicity and weak phonon–phonon interactions are indicated by a low Grüneisen parameter, which is advantageous for high lattice thermal conductivity. Stronger anharmonicity, increased phonon scattering, and therefore decreased thermal conductivity are suggested by a higher Grüneisen value. The following empirical connection can be used to estimate the elastic Grüneisen parameter γ_e of KBi_3 using Poisson's ratio (v):[62]

$$\gamma_e = \frac{3(1+v)}{2(2-3v)} \quad (19)$$

According to Table 3, the elastic Grüneisen parameter (γ_e) for KBi_3 is estimated to be 2.23. According to Slack,[63] the Grüneisen parameter is strongly correlated with lattice thermal conductivity, where higher values of γ_e suggest enhanced phonon–phonon scattering and, consequently, reduced thermal conductivity. The calculated γ_e of KBi_3 is 2.23, which is lower than that of KBi_2 but higher than $RbBi_2$,[9] as presented in Table 3. A relatively higher γ_e value generally reflects stronger anharmonic lattice vibrations and enhanced phonon scattering, characteristics that are closely linked to reduced lattice thermal conductivity—an essential factor governing thermal transport in crystalline solids.[15] Therefore, the elevated γ_e of KBi_3 suggests

Table 3 Summary of selected thermophysical properties of KBi_3 in comparison with related Bi-based compounds. Listed values including density ρ, (in g cm^{-3}), velocitiesv_l, v_t, v_m (in m s^{-1}), melting temperature T_m (in K), Debye temperature θ_D (in K), Grüneisen parameter γ_e and minimum thermal conductivity κ_{min} (in W m^{-1} K^{-1})

Compounds	ρ	v_l	v_t	v_m	T_m	θ_D	γ_e	κ_{min}	Ref.
KBi_3	10.57	2842.196	1323.979	1490.873	968.50	143.72	2.23	0.34	This[a]
KBi_2	7.02	2210.12	890.01	1008.71	745.28	91.05	2.75	0.13	9
$RbBi_2$	7.41	2671.59	1497.18	1659.41	853.99	147.65	1.60	0.20	9

[a] Refers to our theoretical investigation.

a favorable lattice dynamic environment that could support strong electron–phonon interactions, making it a promising candidate for efficient thermal and electronic transport applications.

Lattice thermal conductivity (κ_l), which measures heat transfer through lattice vibrations under a thermal gradient, is a crucial metric for evaluating material performance in high-temperature applications. Thermal barrier coatings (TBCs) are an example of technologies where this characteristic is essential. For intermetallic compounds like materials like KBi_3, low κ_l can be advantageous in maintaining thermal stability and minimizing thermal losses, while in contrast, high κ_l is typically preferred in thermal management systems—such as heat sinks—for efficient heat dissipation. Due to its moderate anharmonicity and distinctive thermal transport properties, KBi_3 exhibits potential for applications where controlled thermal conduction is required to enhance device performance and energy efficiency. To estimate κ_l as a function of temperature, Slack's[63] model is used. The expression of κ_l is as follows:

$$\kappa_l = A(\gamma_e)\frac{M_{av}\theta_D{}^3\delta}{\gamma^2 n^{2/3} T} \quad (20)$$

here, θ_D represents the Debye temperature, M_{av} denotes the average atomic mass, δ is the cube root of the average atomic volume, and γ_e corresponds to the elastic Grüneisen parameter. The factor $A(\gamma_e)$ due to Julian[17] is calculated as

$$A(\gamma_e) = \frac{5.720 \times 10^7 \times 0.849}{2 \times (1 - 0.514/\gamma_e + 0.228/\gamma_e{}^2)} \quad (21)$$

For intermetallic compounds like KBi_3, low can be advantageous in maintaining thermal stability and minimizing thermal losses, while in contrast, high is typically preferred in thermal management systems—such as heat sinks—for efficient heat dissipation. Due to its moderate anharmonicity and distinctive thermal transport properties, KBi_3 exhibits potential for applications where controlled thermal conduction is required to enhance device performance and energy efficiency.

Fig. 2 shows temperature dependence of the lattice thermal conductivity thermal conductivity of KBi_3, showing a decrease with increasing temperature due to enhanced phonon–phonon scattering. The calculated κ_l reaches ~1.16 W m^{-1} K^{-1} at 300 K, indicating low thermal transport efficiency. The large mass contrast between K (~39 u) and Bi (~209 u) splits vibrational branches and enhances acoustic–optical phonon scattering. Bi-dominated low-frequency modes depress sound speeds; together with an elevated Grüneisen parameter (γ_e) these features rationalize the low κ_l *via* strong Umklapp scattering. The lack of a clean acoustic–optical gap in the dispersion facilitates additional scattering channels, explaining the monotonic decline of κ_l and placing KBi_3 among phonon-damped metallic conductors suitable for thermal-management coatings.

Minimum thermal conductivity, k_{min} is the minimum saturating value of a material's thermal conductivity above θ_D. It is important to note that k_{min} is independent of the presence of defects inside the crystal. This is due to phonon transport over larger distances than interatomic spacing and in high temperatures being affected by these defects, thereby reducing the phonon mean free path considerably below this length scale. Based on Debye's concept, Clarke [84] developed the formula for determining a compound's minimum thermal conductivity, k_{min} at high temperatures:

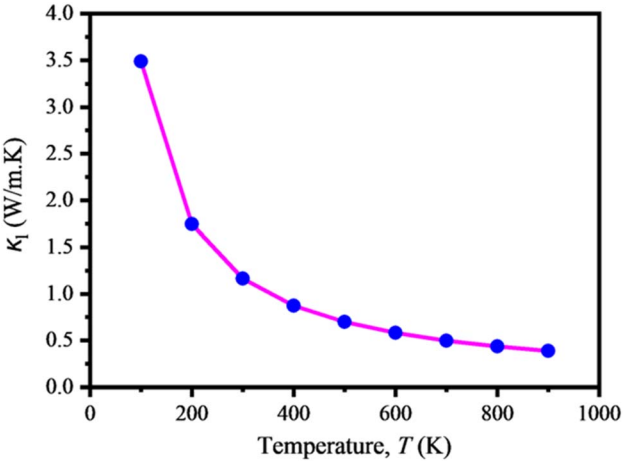

Fig. 2 Temperature dependent lattice thermal conductivity of KBi_3.

$$k_{min} = k_B v_a \left(\frac{M}{n_a \rho N_A}\right)^{-2/3} \quad (22)$$

where, k_B represents the Boltzmann's constant, v_a is the mean sound velocity, M is the molecular mass and n_a is the number of atoms per molecule. The calculated k_{min} for KBi_3 is 0.34 W m^{-1} K^{-1} (Table 3), which is higher than that of KBi_2 and $RbBi_2$,[9] indicating relatively reduced phonon scattering in KBi_3. Nevertheless, this value remains significantly lower than the typical ideal threshold of 1.25 W m^{-1} K^{-1} considered for efficient thermal barrier materials.[16] Low thermal conductivity in conductors often indicates strong phonon scattering, which enhances electron–phonon interactions—an important aspect for optimizing thermal management and improving the performance of optoelectronic devices.[64] Thus, the low k_{min} of KBi_3 supports its potential as a phonon-mediated conductor with efficient lattice vibration damping which enhances electron–phonon interactions.

3.2 Phonon dynamics

In crystalline materials, phonon characteristics are essential. In the Brillouin zone, the phonon dispersion spectra show how phonon energy changes along high-symmetry directions with the wave vector (q). Moreover, the phonon density of states (DOS) and the electron–phonon interaction function are closely connected. Phonon dispersion spectra and phonon DOS have an impact on a number of material properties, both directly and indirectly.[65] Phase transitions, vibrational contributions to a material's thermal characteristics, and structural stability are all revealed by the phonon dispersion spectra (PDS).[66] The phonon dispersion spectra of KBi_3 along the high-symmetry directions of the Brillouin zone (BZ) were computed using the

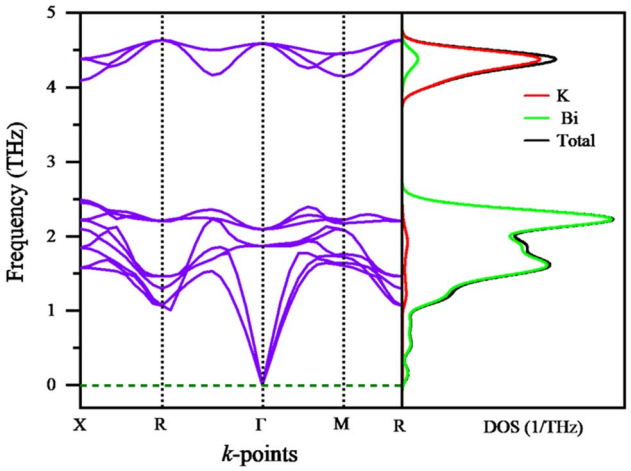

Fig. 3 Phonon dispersion curves and corresponding phonon density of states (DOS) of KBi_3.

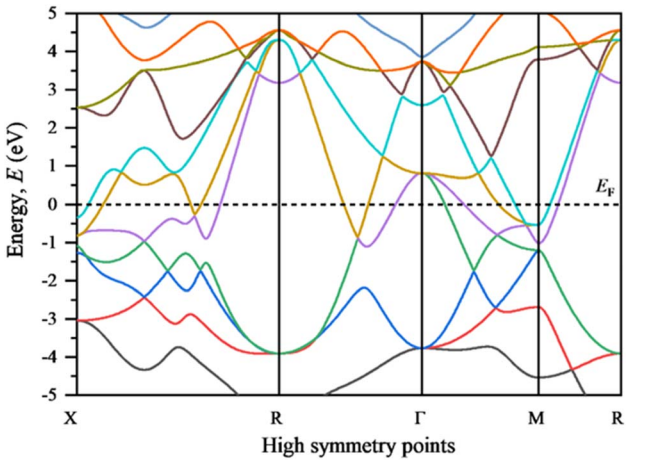

Fig. 4 Electronic band structure of KBi_3 along high-symmetry directions in the Brillouin zone.

linear response approach based on density functional perturbation theory (DFPT).[10,67,68] The dynamic stability of KBi_3 is confirmed by the PDS's lack of negative frequencies near the gamma point,[67] as seen in Fig. 3. Acoustic branches, which result from the coherent motion of atoms moved out of their equilibrium positions, are represented by the bottom part of the dispersion spectrum. The compound's dynamic stability is further confirmed by the acoustic modes exhibiting zero frequency at the Γ point.[68] On the other hand, optical branches that sustain non-zero frequencies at the Γ point make up the upper part of the dispersion spectrum. The optical characteristics of crystals are mostly influenced by optical branches. The absence of a phonon gap between the optical and acoustic branches further suggests a strong connection between them, which lowers the lattice thermal conductivity (κ_l). Additionally, the calculated total and phonon partial density of states (PDOS) are shown in the right panel of Fig. 3. Acoustic modes, lower optical modes, and higher optical modes are the three parts that make up the PDOS. According to the phonon partial density of states (PDOS), the heavier Bi atom dominates the low-frequency vibrations whilst the lighter K atoms contribute significantly to the high-frequency vibrations. In addition to confirming the dynamical stability of KBi_3, the phonon dispersion and DOS data show how each atomic species contributes differently to the vibrational dynamics of the material, which in turn affects its thermal conductivity, heat capacity, and thermal expansion behavior.[44] Soft acoustic branches and sizable Grüneisen parameters reveal appreciable anharmonicity, providing a microscopic origin for the reduced lattice thermal conductivity and confirming that KBi_3 remains dynamically and thermodynamically stable over the relevant temperature range.

3.3 Electronic band structure and density of states

Almost all key physical properties of solid materials are governed by the behavior of valence and conduction electrons, which in turn is dictated by the electronic energy dispersion E(k) throughout the Brillouin zone. This energy variation with momentum outlines the electronic band structure. We have calculated the electronic band structure of KBi_3 based on its optimized crystal structure. The band dispersion along high-symmetry paths in the Brillouin zone, as well as the total and partial density of states (TDOS and PDOS), are shown in Fig. 4 and 5. The Fermi energy, E_F, is set at zero in the plots for clarity. From the band structure, it is evident that several electronic bands intersect the Fermi level, confirming the metallic nature of KBi_3. The slope of the energy bands with respect to momentum gives the group velocity of charge carriers.

A finite TDOS at the Fermi level further confirms its metallic character. Significant hybridization is observed near E_F, primarily from Bi-6p states, which dominate both the

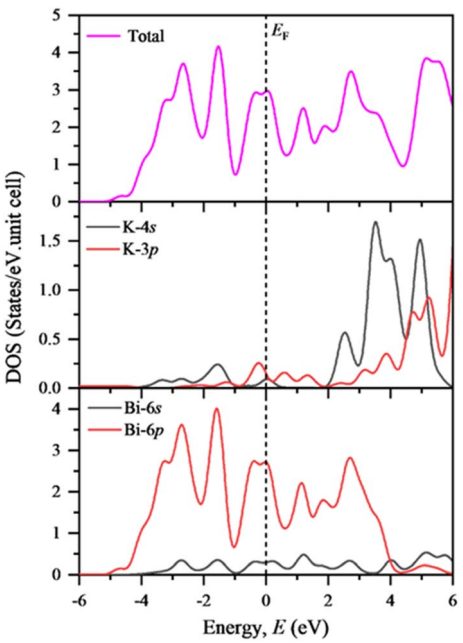

Fig. 5 Total and partial electronic density of states (DOS) of KBi_3.

conduction and valence bands, whereas K states contribute much less, indicating a more ionic character of K in the lattice. The relatively weak participation of K atoms may also explain the observed softness and ductility of KBi_3. Several prominent peaks appear in the TDOS at different energy levels, which are expected to influence optical transitions and transport behavior. Notably, the pronounced peak near the Fermi level highlights the potential of KBi_3 for electronic and transport applications.[8,64] Furthermore, its metallic character, combined with the high reflectivity observed in the optical response, makes KBi_3 promising for infrared coatings and optoelectronic devices.[10] The low C_{44} and the hierarchy $G \ll B$ indicate facile shear relative to compression, consistent with Bi-6p-dominated, delocalized bonding at E_F. The PDOS shows minor K weight at E_F, implying weak K–Bi directionality; this favors bond bending over bond stretching (Kleinman $\zeta \approx 0.75$), a microscopic origin of the observed softness and ductility. Anisotropic band slopes near E_F further correlate with direction-dependent shear compliance and the positive Cauchy pressure, typical of metal-like bonding that supports plasticity. The high and relatively flat density of states around E_F indicates a large reservoir of itinerant carriers, which is favorable for metallic conduction and underpins the strong Drude-like optical response.

3.4 Thermodynamic properties

Functional materials like KBi_3 are often subjected to varying thermal conditions in practical applications. Therefore, understanding the temperature-dependent behavior of their thermodynamic properties is crucial for assessing their potential in device and engineering applications. In this study, the temperature-dependent thermodynamic properties of KBi_3 have been investigated using the quasi-harmonic Debye approximation (QHDA). This approach is a lattice dynamical model that allows for the estimation of thermal effects as a function of temperature by assuming that the harmonic approximation holds at each volume point, with the lattice constant varying accordingly. We studied different thermodynamic properties under 0 GPa pressure and temperatures ranging from 0 to 900 K, without surpassing its melting temperature (T_m), using the generalized gradient approximation (GGA).

It is evident from Fig. 6(a) that temperature reduces the bulk modulus. As temperature rises at various pressures, the bulk modulus value exhibits a diminishing linear trend. This behavior aligns with the third law of thermodynamics and is attributed to the thermal softening of the material's lattice structure. In this study, the bulk modulus was calculated using the quasi-harmonic Debye model and the Gibbs2 code ($B = 51.2$ GPa), agreeing well with the values found while calculating structural characteristics.

Fig. 6(b) illustrates the variation of heat capacities (C_p) and (C_v) with temperature at zero pressure. As observed, both (C_p) and (C_v) increase rapidly up to approximately 200 K. Beyond this temperature, the anharmonic effects on C_v begin to diminish, and it gradually approaches a constant value, the Dulong–Petit limit[69] ($C_v = 3\ nR = 99.76785$ J mol^{-1}K^{-1}), which is characteristic of all solids at high temperatures. Similarly, C_P continues to increase monotonically beyond 200 K. In the low-temperature regime, both (C_p) and (C_v) follow the Debye T^3-law, indicative of phonon-dominated thermal behavior. At higher temperatures, whileC_v levels off near the classical limit, C_p continues to rise above C_v, a divergence primarily attributed to the effects of thermal expansion under constant pressure. This behavior is especially pronounced in materials exhibiting significant thermal expansion. The smooth, monotonic evolution of heat capacity with temperature, without anomalies, corroborates the absence of phase instabilities and supports the suitability of KBi_3 for operation over a broad thermal window.

Fig. 6(c) shows the variation of Debye temperature (θ_D) as a function of temperature at zero pressure. A crucial characteristic of crystals that affects their thermal characteristics is their Debye temperature (θ_D). Atoms in a solid vibrate when the temperature rises above absolute zero. This vibrational maximum is represented by θ_D, which also indicates the material's hardness or rigidity.[70] The Debye temperature decreases relatively slowly as temperature rises, as shown in Fig. 6(c). This decrease reflects the reduction in lattice stiffness due to thermal vibrations, which is consistent with the corresponding decrease in the bulk modulus. At zero temp. and ambient pressure the value of θ_D of KBi_3 is 175.66 K, which agrees well with our calculated values using elastic constants.

Thermal expansion measurement yields valuable insights into the interatomic forces present in crystals. Helmholtz free energy and crystal lattice anharmonicity are related to it. Thermal expansion is linked to the anharmonicity of the crystal lattice interaction potential.[70] The volume thermal expansion coefficient α, shown in Fig. 6(d), increases significantly with temperature, especially above room temperature. This is indicative of the relatively soft nature of the KBi_3 lattice, possibly due to its weak interatomic bonding characteristics. The thermal expansion behavior is typical for metals and van der Waals-type layered compounds.

3.5 Optical properties

The optical properties of a material are essential for understanding its interaction with incident electromagnetic radiation and play a critical role in evaluating its suitability for optoelectronic and photovoltaic device applications. In this context, the response of a compound across the infrared, visible, and ultraviolet (UV) regions of the electromagnetic spectrum is particularly significant. To investigate the optical behavior of KBi_3, several frequency-dependent optical parameters were computed, including the real and imaginary parts of the dielectric function, $\varepsilon_1(\omega)$ and $\varepsilon_2(\omega)$, respectively; the refractive index $n(\omega)$; extinction coefficient $k(\omega)$; the energy loss function $L(\omega)$; the real and imaginary parts of the optical conductivity, $\sigma_1(\omega)$ and $\sigma_2(\omega)$; the reflectivity $R(\omega)$; and the absorption coefficient $\alpha(\omega)$. These parameters were calculated for photon energies up to 14 eV, with the electric field polarization vector aligned along the [100] crystallographic direction, as shown in Fig. 7. According to the electronic band structure analysis, KBi_3 exhibits a metallic nature. Consequently, it is necessary to include a Drude-like intraband correction in the optical

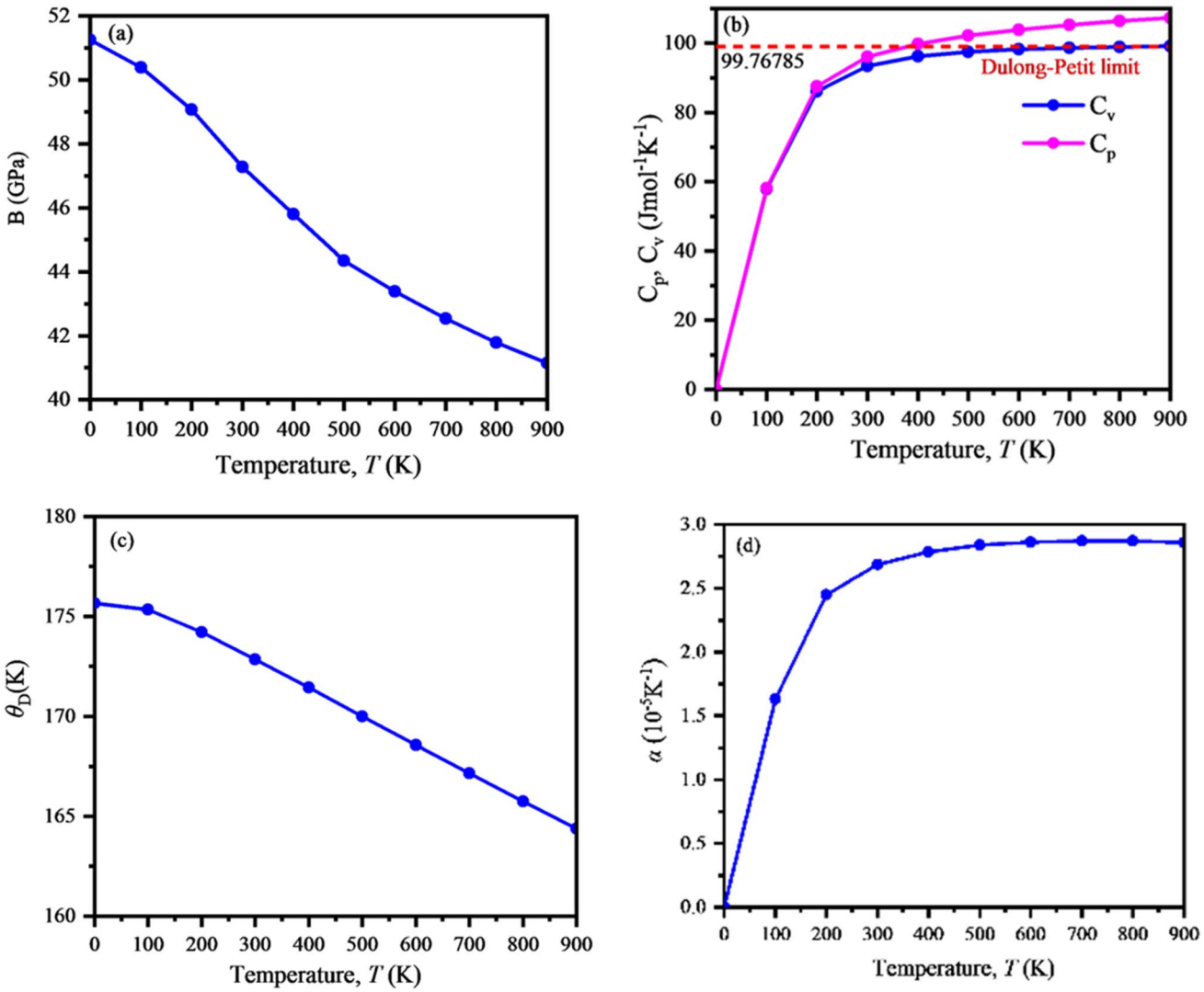

Fig. 6 Temperature dependence of thermodynamic properties of KBi_3: (a) bulk modulus B, (b) heat capacities C_p and C_v, (c) Debye temperature θ_D and (d) volumetric thermal expansion coefficient α.

calculations. For this purpose, a screened plasma energy of 10 eV and a Drude damping constant of 0.05 eV were employed, following established approaches.[10,71] The optical parameters of a material can be derived from its complex dielectric function, $\varepsilon(\omega)$, which is primarily governed by both intraband and interband electronic transitions. In this study, indirect interband transitions were neglected, as they involve phonon participation and typically exhibit a significantly lower scattering cross-section compared to direct transitions, where momentum conservation does not require phonon assistance.[72] Because KBi_3 is metallic with Bi-6p carriers, intraband (Drude) processes dominate at low $\hbar\omega$, producing high IR reflectivity (~70%) and a large static refractive index—desirable for IR-reflective/heat-shield coatings where radiative heat loss must be minimized. Unlike semiconductors, the finite DOS at E_F yields low contact resistance and robust photoconductive response at low photon energies, making KBi_3 a practical metallic electrode/flexible conductor; conversely, the absence of a band gap means broadband absorption arises from higher-energy interband transitions rather than a tunable band edge.

Fig. 7(a) illustrates the calculated real ($\varepsilon_1(\omega)$) and imaginary ($\varepsilon_2(\omega)$) parts of the dielectric function. The static dielectric constant $\varepsilon_1(0)$, a key optical parameter, is generally inversely related to the material's band gap. As shown in Fig. 7(a), the investigated compound demonstrates metallic behavior, consistent with its electronic band structure and total density of states (TDOS) (Fig. 4 and 5). Furthermore, the characteristic metallic response is evident in regions where $\varepsilon_1(\omega)$ becomes negative, indicating strong reflectivity typical of metals.

The refractive index is a complex optical parameter defined as $N(\omega) = n(\omega) + ik(\omega)$, where $n(\omega)$ is the real part representing the phase velocity of light in the material, and $k(\omega)$ is the imaginary part, known as the extinction coefficient, which quantifies the material's attenuation of the electromagnetic wave. The calculated spectra of $n(\omega)$ and $k(\omega)$ for KBi_3 are presented in Fig. 7(b). The refractive index attains its maximum at zero photon energy and gradually decreases with increasing

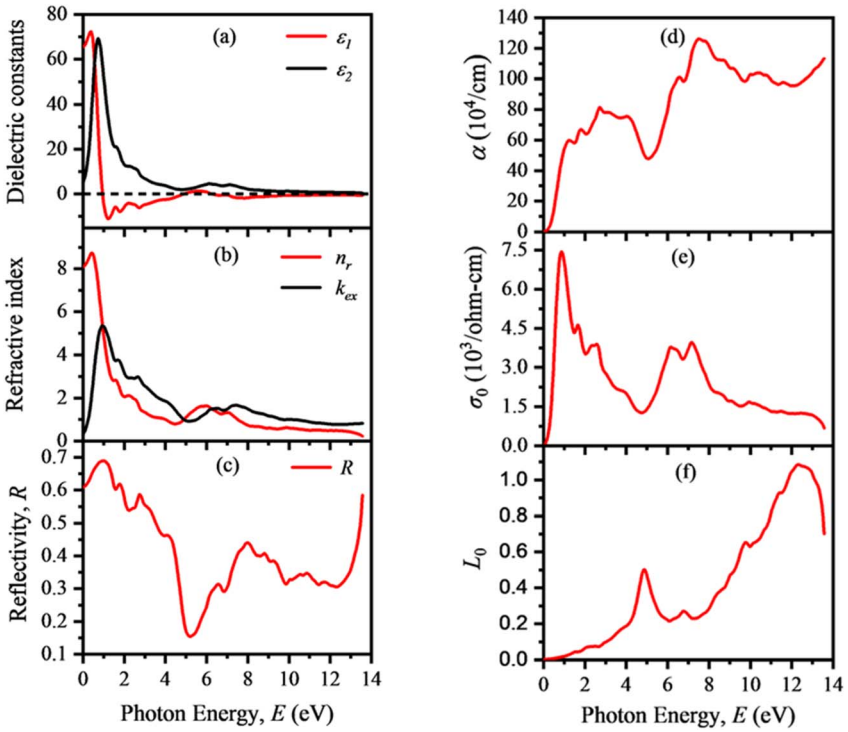

Fig. 7 Photon-energy-dependent optical response of KBi_3: (a) real ε_1 and imaginary part ε_2 of dielectric function, (b) refractive index n_r and extinction coefficient k_{ex}, (c) reflectivity R (d) absorption α (e) optical conductivity σ_0 and (f) loss function L.

photon energy. The peak in $n(\omega)$ typically arises due to electronic transitions from the valence to the conduction band. A higher extinction coefficient indicates a stronger light absorption capability. Notably, KBi_3 exhibits a high refractive index at low photon energies, particularly within the infrared to visible regions, which has significant practical implications. Materials with high refractive indices are highly desirable for applications in optoelectronic display devices and light-emitting technologies.

Reflectivity, another crucial optical parameter, is important for evaluating the potential of a material as a coating in various optical applications. The reflectivity spectrum of KBi_3, displayed in Fig. 7(c), spans the energy range of 0 to 14 eV. Interestingly, KBi_3 exhibits high reflectivity in the infrared region, with a reflectivity of around 70%. High infrared reflectivity reduces radiative heat losses, enhancing thermal insulation and stability in optoelectronic devices.[11]

The absorption coefficient provides insights into the solar energy conversion efficiency of a material and also reflects its electronic nature—whether metallic, semiconducting, or insulating. As shown in Fig. 7(d), KBi_3 exhibits significant absorption beginning from zero photon energy. The initial optical absorption is attributed to free electron transitions within the conduction band. A prominent absorption peak occurs at approximately 7.50 eV. This is followed by a sharp decline near 12.0 eV, which corresponds to the energy loss peak.

The photoconductivity spectrum, shown in Fig. 7(e), begins at zero photon energy, confirming the metallic character of KBi_3. As photon energy increases, the compound's photoconductivity rises to its maximum, then steadily falls as energy climbs further, tending to zero at about 14 eV.

The energy loss function $L(\omega)$, shown in Fig. 7(f), is associated with the energy loss of fast electrons traversing the material and provides information on plasmonic excitations. It is also closely related to the material's absorption and reflection behavior. The loss spectrum reflects collective charge oscillations (plasmons) induced by photon absorption. The peak in $L(\omega)$ appears at 12.4 eV, representing the bulk screened plasma frequency of the material. This sharp peak indicates a sudden drop in both reflectivity and absorption (see Fig. 7(c) and (d)). Above this energy, KBi_3 becomes transparent and shifts its optical response from metallic to dielectric. The plasmon energy corresponds to the energy at which the real part of the dielectric constant $\varepsilon_1(\omega)$ crosses zero, as shown in Fig. 7(a). The onset and magnitude of the optical absorption correlate well with the interband transitions identified in the band structure, ensuring that the main loss channels can be directly linked to specific electronic states.

The metallic character of KBi_3, dominated by Bi-6p states at the Fermi level, governs both its mechanical and optical responses. The continuous density of states at E_F ensures a high density of free carriers, producing Drude-type intraband transitions that yield high infrared reflectivity and large static dielectric response—attributes required for infrared mirrors and heat-shield coatings. In contrast to semiconductors, where a band gap limits carrier availability, the metallic KBi_3 enables efficient electron transport and minimal contact resistance, suggesting its utility as a flexible metallic electrode or interconnect material in optoelectronic modules. Furthermore, the

non-directional metallic bonding between K and Bi underlies its ductility and mechanical flexibility, important for deformable coating layers that can withstand operational stress.

4 Conclusion

In this work, we have performed a comprehensive first-principles investigation of the structural, elastic, electronic, thermodynamic, phonon, and optical properties of cubic KBi_3 to evaluate its suitability for advanced functional applications. The optimized lattice parameters are consistent with available data, confirming the reliability of our theoretical approach. The mechanical analysis reveals that KBi_3 is mechanically stable and exhibits notable softness and ductility, supported by its low elastic moduli, high B/G ratio, positive Cauchy pressure, and high machinability index. These features suggest good mechanical flexibility and ease of processing, making the compound promising for flexible electronic components and deformable metal contacts. Thermodynamic modeling predicts a relatively low Debye temperature, moderate melting point, and low lattice thermal conductivity, indicating a soft lattice with enhanced phonon scattering mechanisms. These characteristics are beneficial for thermal-management coatings and phonon-coupled optoelectronic systems. The electronic band structure and density-of-states analyses confirm metallic behavior dominated by Bi-6*p* states at the Fermi level, implying high carrier mobility and suitability for plasmonic, low-resistance interconnect, and metallic electrode applications. The optical spectra demonstrate strong reflectivity in the infrared regime, a high refractive index, and pronounced absorption across the visible-UV range. These distinctive optical responses highlight the potential of KBi_3 for infrared-reflective coatings, radiative heat-shielding materials, photonic devices, and high-frequency electromagnetic applications. The phonon dispersion calculations show no negative frequencies, confirming dynamical stability and reliable vibrational behavior.

Overall, this study provides the first complete theoretical understanding of KBi_3 and identifies it as a promising multi-functional metallic material with technological potential in flexible electronic contacts, plasmonic systems, infrared-shielding coatings, thermal-management layers, and broad-band optoelectronic and photonic devices. Experimental synthesis and device-scale testing are encouraged to further validate and exploit these properties.

Author contributions

M. M. Rabbi: methodology, software, formal analysis, data curation, visualization, writing – original draft, Mst A. Khatun: conceptualization, supervision, validation, formal analysis, writing – review & editing.

Conflicts of interest

The authors declare that they have no known competing financial interests or personal relationships that could have appeared to influence the work reported in this paper.

Data availability

Upon reasonable request, the associated author will make the data sets created during the current study available.

References

1 P. Villars, K. Cenzual, *Pearsons crystal data: crystal structure database for inorganic compounds*, No Title (2007).
2 E. A. Riesel, T. Mackey, H. Nilforoshan, M. Xu, C. K. Badding, A. B. Altman, J. Leskovec and D. E. Freedman, Crystal structure determination from powder diffraction patterns with generative machine learning, *J. Am. Chem. Soc.*, 2024, **146**, 30340–30348.
3 T. B. Massalski, J. L. Murray, L. H. Bennett and H. Baker, *Binary Alloy Phase Diagrams*, American society for metals, Metals Park, OH, 1986.
4 J. P. Walsh, S. M. Clarke, Y. Meng, S. D. Jacobsen and D. E. Freedman, Discovery of $FeBi_2$, *ACS Cent. Sci.*, 2016, **2**, 867–871.
5 J. P. Walsh, S. M. Clarke, D. Puggioni, A. D. Tamerius, Y. Meng, J. M. Rondinelli, S. D. Jacobsen and D. E. Freedman, $MnBi_2$: A Metastable High-Pressure Phase in the Mn–Bi System, *Chem. Mater.*, 2019, **31**, 3083–3088.
6 E. Havinga, H. Damsma and M. Van Maaren, Oscillatory dependence of superconductive critical temperature on number of valency electrons in Cu3Au-type alloys, *J. Phys. Chem. Solids*, 1970, **31**, 2653–2662.
7 R. Ramesh and D. G. Schlom, Creating emergent phenomena in oxide superlattices, *Nat. Rev. Mater.*, 2019, **4**, 257–268.
8 H. Li, M. Ikeda, A. Suzuki, T. Taguchi, Y. Zhang, H. Goto, R. Eguchi, Y.-F. Liao, H. Ishii and Y. Kubozono, Pressure dependence of superconductivity in alkali-Bi compounds KBi_2 and $RbBi_2$, *Phys. Chem. Chem. Phys.*, 2022, **24**, 7185–7194.
9 J. Hassan, M. Masum and S. Naqib, A comparative ab-initio investigation of the physical properties of cubic Laves phase compounds XBi_2 (X= K, Rb), *Comput. Condens. Matter*, 2024, **39**, e00905.
10 R. Saniz, L.-H. Ye, T. Shishidou and A. Freeman, Structural, electronic, and optical properties of $NiAl_3$: first-principles calculations, *Phys. Rev. B:condens. Matter Mater. Phys.*, 2006, **74**, 014209.
11 H. K. Woo, K. Zhou, S. Kim, A. Manjarrez, M. J. Hoque, T. Seong and L. Cai, Visibly transparent and infrared reflective coatings for personal thermal management and thermal camouflage, *Adv. Funct. Mater.*, 2022, **32**, 2201432.
12 X.-P. Wei, Y.-H. Zhou and Y.-L. Zhang, First-Principles Study the Electronic and Thermodynamic Properties for CoBi3 Superconductor, *J. Supercond. Novel Magn.*, 2016, **29**, 1203–1211.
13 D. Shao, X. Luo, W. Lu, L. Hu, X. Zhu, W. Song, X. Zhu and Y. Sun, Spin-orbit coupling enhanced superconductivity in Bi-rich compounds ABi_3 (A = Sr and Ba), *Sci. Rep.*, 2016, **6**, 21484.

14 T. Kinjo, S. Kajino, T. Nishio, K. Kawashima, Y. Yanagi, I. Hase, T. Yanagisawa, S. Ishida, H. Kito and N. Takeshita, Superconductivity in $LaBi_3$ with $AuCu_3$-type structure, *Supercond. Sci. Technol.*, 2016, **29**, 03LT02.

15 K. S. Rana, D. Sarkar, Nidhi, A. Singh, C. Bera, K. Biswas and A. Soni, Ultralow lattice thermal conductivity in complex structure $Cu_{26}V_2Sn_6Se_{32}$ due to interaction of low-frequency acoustic-optical phonons, *Phys. Rev. B*, 2024, **109**, 115202.

16 I. Ahmed, F. Parvin, A. Islam and M. Kashem, Inverse-perovskites Sc_3GaX (X= B, C, N): a comprehensive theoretical investigation at ambient and elevated pressures, *Comput. Condens. Matter*, 2023, **35**, e00808.

17 C. L. Julian, Theory of heat conduction in rare-gas crystals, *Phys. Rev.*, 1965, **137**, A128.

18 P. Blaha, K. Schwarz, G. K. Madsen, D. Kvasnicka and J. Luitz, WIEN2K, an Augmented Plane Wave + Local Orbitals Program for Calculating Crystal Properties, edited by K, *Schwarz Vienna Univ. Technol.*, Austria, 2001.

19 J. P. Perdew, K. Burke and M. Ernzerhof, Generalized gradient approximation made simple, *Phys. Rev. Lett.*, 1996, **77**, 3865.

20 J. P. Perdew, A. Ruzsinszky, G. I. Csonka, O. A. Vydrov, G. E. Scuseria, L. A. Constantin, X. Zhou and K. Burke, Restoring the density-gradient expansion for exchange in solids and surfaces, *Phys. Rev. Lett.*, 2008, **100**, 136406.

21 S. J. Clark, M. D. Segall, C. J. Pickard, P. J. Hasnip, M. I. Probert, K. Refson, M. C. Payne and Z. Für, First principles methods using CASTEP, *Z. Kristallogr. Cryst. Mater.*, 2005, **220**, 567–570.

22 S. Hadji, A. Bouhemadou, K. Haddadi, D. Cherrad, R. Khenata, S. Bin-Omran and Y. Al-Douri, Elastic, electronic, optical and thermodynamic properties of Ba3Ca2Si2N6 semiconductor: first-principles predictions, *Phys. B Condens. Matter*, 2020, **589**, 412213.

23 S. Touam, R. Belghit, R. Mahdjoubi, Y. Megdoud, H. Meradji, M. S. Khan, R. Ahmed, R. Khenata, S. Ghemid and D. P. Rai, First-principles computations of $Y_xGa_{1-x}As$-ternary alloys: a study on structural, electronic, optical and elastic properties, *Bull. Mater. Sci.*, 2020, **43**, 22.

24 F. Parvin and S. Naqib, Structural, elastic, electronic, thermodynamic, and optical properties of layered BaPd2As2 pnictide superconductor: a first principles investigation, *J. Alloys Compd.*, 2019, **780**, 452–460.

25 A. Chowdhury, M. Ali, M. Hossain, M. Uddin, S. Naqib and A. Islam, Predicted MAX phase Sc_2InC: dynamical stability, vibrational and optical properties, *Phys. Status Solidi B*, 2018, **255**, 1700235.

26 M. Ali, M. Nasir, M. Khatun, A. Islam and S. Naqib, An ab initio investigation of vibrational, thermodynamic, and optical properties of Sc_2AlC MAX compound, *Chin. Phys. B*, 2016, **25**, 103102.

27 M. Roknuzzaman, M. Hadi, M. Abden, M. Nasir, A. Islam, M. Ali, K. Ostrikov and S. Naqib, Physical properties of predicted Ti_2CdN versus existing Ti_2CdC MAX phase: An ab initio study, *Comput. Mater. Sci.*, 2016, **113**, 148–153.

28 M. Hossain and S. Naqib, Structural, elastic, electronic, andoptical properties of layered TiNX (X= F, Cl, Br, I) compounds: a density functional theory study, *Mol. Phys.*, 2020, **118**, e1609706.

29 A. Otero-de-la-Roza and V. Luaña, Gibbs2: A new version of the quasi-harmonic model code. I. Robust treatment of the static data, *Comput. Phys. Commun.*, 2011, **182**, 1708–1720.

30 M. Blanco, E. Francisco and V. Luana, GIBBS: isothermal-isobaric thermodynamics of solids from energy curves using a quasi-harmonic Debye model, *Comput. Phys. Commun.*, 2004, **158**, 57–72.

31 E. Francisco, M. Blanco and G. Sanjurjo, Atomistic simulation of SrF_2 polymorphs, *Phys. Rev. B:condens. Matter Mater. Phys.*, 2001, **63**, 094107.

32 E. Francisco, J. Recio, M. Blanco, A. M. Pendás and A. Costales, Quantum-mechanical study of thermodynamic and bonding properties of MgF_2, *J. Phys. Chem. A*, 1998, **102**, 1595–1601.

33 V. G. Tyuterev and N. Vast, Murnaghan's equation of state for the electronic ground state energy, *Comput. Mater. Sci.*, 2006, **38**, 350–353.

34 Z. Liu, D. Gall and S. Khare, Electronic and bonding analysis of hardness in pyrite-type transition-metal pernitrides, *Phys. Rev. B*, 2014, **90**, 134102.

35 K. Akter, F. Parvin, M. Hadi and A. Islam, Insights into the predicted Hf_2SN in comparison with the synthesized MAX phase Hf_2SC: A comprehensive study, *Comput. Condens. Matter*, 2020, **24**, e00485.

36 A. Aliakbari, P. Amiri and A. G. Dezfuli, Stability and physical properties of yttrium-based new MAX phases Y_2AX (A= Al, Si, Ga, and Ge; X= C and N): a first-principles prediction, *Appl. Phys. A*, 2023, **129**, 476.

37 M. Ali, M. Hossain, M. Uddin, A. Islam, D. Jana and S. Naqib, DFT insights into new B-containing 212 MAX phases: Hf_2AB_2 (A= In, Sn), *J. Alloys Compd.*, 2021, **860**, 158408.

38 M. Rabbi and M. Khatun, Unlocking the optoelectronic and thermoelectric properties of Ba2ZnTeO6: a promising double perovskite for sustainable energy harvesting technologies, *Opt. Quant. Electron.*, 2025, **57**, 1–31.

39 A. Candan, G. Uğur, Z. Charifi, H. Baaziz and M. Ellialtıoğlu, Electronic structure and vibrational properties in cobalt-based full-Heusler compounds: A first principle study of Co_2MnX (X = Si, Ge, Al, Ga), *J. Alloys Compd.*, 2013, **560**, 215–222.

40 H. Ledbetter and E. Naimon, Elastic properties of metals and alloys. II. Copper, *J. Phys. Chem. Ref. Data*, 1974, **3**, 897–935.

41 W. Voigt, *Lehrbuch der Kristallphysik*, Teubner, 1928.

42 A. Reuß, Berechnung der fließgrenze von mischkristallen auf grund der plastizitätsbedingung für einkristalle, *Z. Angew. Math. Mech.*, 1929, **9**, 49–58.

43 R. Hill, The elastic behaviour of a crystalline aggregate, *Proc. Phys. Soc.*, 1952, **65**, 349.

44 M. Rabbi, M. Mia, S. Saif, U. Ahmed, M. Hossain, M. Uddin and M. Ali, DFT Prediction of Double Perovskites $A_2B'RhCl_6$ (A= Cs/Rb; B′= Na/K) for Green Energy Technology, *Comput. Condens. Matter*, 2025, e01093.

45 C. Kittel, *Introduction to Solid State Physics*, 8th edn, (2021).

46 A. Yıldırım, H. Koç and E. Deligöz, First-principles study of the structural, elastic, Electronic, Optical, and Vibrational Properties of Intermetallic Pd_2Ga, *Chin. Phys. B*, 2012, **21**, 03710.

47 A. F. Young, C. Sanloup, E. Gregoryanz, S. Scandolo, R. J. Hemley and H. Mao, Synthesis of novel transition metal nitrides IrN 2 and OsN_2, *Phys. Rev. Lett.*, 2006, **96**, 155501.

48 S. Pugh, XCII. Relations between the elastic moduli and the plastic properties of polycrystalline pure metals, *Philos. Mag.*, 1954, **45**, 823–843.

49 G. Vaitheeswaran, V. Kanchana, R. S. Kumar, A. Cornelius, M. Nicol, A. Svane, A. Delin and B. Johansson, High-pressure structural, elastic, and electronic properties of the scintillator host material K Mg F 3, *Phys. Rev. B:condens. Matter Mater. Phys.*, 2007, **76**, 014107.

50 E. Haque and M. A. Hossain, First-principles study of elastic, electronic, thermodynamic, and thermoelectric transport properties of TaCoSn, *Results Phys.*, 2018, **10**, 458–465.

51 H. Fu, D. Li, F. Peng, T. Gao and X. Cheng, Ab initio calculations of elastic constants and thermodynamic properties of NiAl under high pressures, *Comput. Mater. Sci.*, 2008, **44**, 774–778.

52 D. Pettifor, Theoretical predictions of structure and related properties of intermetallics, *Mater. Sci. Technol.*, 1992, **8**, 345–349.

53 L. Kleinman, Deformation potentials in silicon. I. Uniaxial strain, *Phys. Rev.*, 1962, **128**, 2614.

54 Z. Sun, D. Music, R. Ahuja and J. M. Schneider, Theoretical investigation of the bonding and elastic properties of nanolayered ternary nitrides, *Phys. Rev. B:condens. Matter Mater. Phys.*, 2005, **71**, 193402.

55 L. Vitos, P. A. Korzhavyi and B. Johansson, Stainless steel optimization from quantum mechanical calculations, *Nat. Mater.*, 2003, **2**, 25–28.

56 R. Lincoln, K. Koliwad and P. Ghate, Morse-potential evaluation of second-and third-order elastic constants of some cubic metals, *Phys. Rev.*, 1967, **157**, 463.

57 M. Phasha, P. Ngoepe, H. Chauke, D. Pettifor and D. Nguyen-Mann, Link between structural and mechanical stability of fcc-and bcc-based ordered Mg–Li alloys, *Intermetallics*, 2010, **18**, 2083–2089.

58 K. J. Puttlitz and K. A. Stalter, *Handbook of Lead-free Solder Technology for Microelectronic Assemblies*, CRC Press, 2004.

59 M. Mattesini, R. Ahuja and B. Johansson, Cubic Hf_3N_4 and Zr_3N_4: A class of hard materials, *Phys. Rev. B:Condens. Matter Mater. Phys.*, 2003, **68**, 184108.

60 M. Fine, L. Brown and H. Marcus, Elastic constants versus melting temperature in metals, *Scr. Metall.*, 1984, **18**, 951–956.

61 O. L. Anderson, A simplified method for calculating the Debye temperature from elastic constants, *J. Phys. Chem. Solids*, 1963, **24**, 909–917.

62 V. N. Belomestnykh and E. P. Tesleva, Interrelation between Anharmonicity and Lateral Strain in Quasi-Isotropic Polycrystalline Solids, *Tech. Phys.*, 2004, **49**, 1098–1100.

63 G. A. Slack, The thermal conductivity of nonmetallic crystals, *Solid State Phys.*, 1979, **34**, 1–71.

64 G. Grimvall, *The electron-phonon interaction in metals*, 1981.

65 E. N. Koukaras, G. Kalosakas, C. Galiotis and K. Papagelis, Phonon properties of graphene derived from molecular dynamics simulations, *Sci. Rep.*, 2015, **5**, 12923.

66 Y. Yun, D. Legut and P. M. Oppeneer, Phonon spectrum, thermal expansion and heat capacity of UO2 from first-principles, *J. Nucl. Mater.*, 2012, **426**, 109–114.

67 A. Basak, A. Irfan, M. A. Khatun, M. Rabbi, D. Roy, M. Y. H. Khan, M. Ali, M. F. Rahman and M. A. Rahman, First-principles study of M_4AlC_3 (M = Ti, Zr) MAX phases under hydrostatic pressure: material design for industrial applications, *RSC Adv.*, 2025, **15**, 27210–27237.

68 M. Hadi, M. Rayhan, S. Naqib, A. Chroneos and A. Islam, Structural, elastic, thermal and lattice dynamic properties of new 321 MAX phases, *Comput. Mater. Sci.*, 2019, **170**, 109144.

69 K. Wei, D. Hobbis, H. Wang and G. S. Nolas, Wittichenite Cu_3BiS_3: Synthesis and Physical Properties, *J. Electron. Mater.*, 2018, **47**, 2374–2377.

70 Z. Ech-Charqy, M. Ziati and H. Ez-Zahraouy, Stretch effects on structural, electronic, optical, and thermoelectric features of $LiGeBr_3$: A DFT calculations, *Mod. Phys. Lett. B*, 2023, **37**, 2350187.

71 S. Li, R. Ahuja, M. Barsoum, P. Jena and B. Johansson, Optical properties of Ti_3SiC_2 and Ti_4AlN_3, *Appl. Phys. Lett.*, 2008, **92**, 221907.

72 A. H. Reshak, V. Atuchin, S. Auluck and I. Kityk, First and second harmonic generation of the optical susceptibilities for the non-centro-symmetric orthorhombic$AgCd_2GaS_4$, *J. Phys. Condens. Matter*, 2008, **20**, 325234.